# Vibronic enhancement of excitation energy transport: interplay between local and non-local exciton-phonon interaction

Myeong H. Lee* and Alessandro Troisi

*Department of Chemistry, University of Warwick, Coventry CV4 7AL, UK*

(Dated: February 11, 2017)

## Abstract

It has been reported in recent years that vibronic resonance between vibrational energy of the intramolecular nuclear mode and excitation-energy difference is crucial to enhance excitation energy transport in light harvesting proteins. Here we investigate how vibronic enhancement induced by vibronic resonance is influenced by the details of local and non-local exciton-phonon interaction. We study a heterodimer model with parameters relevant to the light-harvesting proteins with the surrogate Hamiltonian quantum dynamics method in a vibronic basis. In addition, the impact of field-driven excitation on the efficiency of population transfer is compared with the instantaneous excitation, and the effect of multi-mode vibronic coupling is presented in comparison with the coupling to a single effective vibrational mode. We find that vibronic enhancement of site population transfer is strongly suppressed with the increase of non-local exciton-phonon interaction and increasing the number of strongly coupled high-frequency vibrational modes leads to further decrease in vibronic enhancement. Our results indicate that vibronic enhancement is present but may be much smaller than previously thought and therefore care needs to be taken when interpreting its role in excitation energy transport. Our results also suggest that non-local exciton-phonon coupling, which is related to the fluctuation of the excitonic coupling, may be as important as local exciton-phonon coupling and should be included in any quantum dynamics model.

## I. INTRODUCTION

In many photophysical processes there is often a strong mixing of the electronic state with vibrational modes and the role of such strong vibronic coupling in exciton and charge transport has been the focus of many studies in recent years.[1–19] Vibronic coupling has been ascribed to the origin of long-lived coherences observed in two dimensional (2D) electronic spectra of the natural/artificial light harvesting complexes[1–5,16,18,20–22] and the photosystem II reaction centre[6,7] and to the underlying mechanism of ultrafast coherent charge transfer in organic photovoltaic systems[8,9] and ultrafast singlet fission process in pentacene and its derivatives.[10–13] The vibrational degrees of freedom (DOFs) that interact with the electronic DOFs in photosynthetic complexes are either the vibrations of the environment (e.g., protein scaffold, solvent medium, and inter-pigment vibrations of low-frequency modes) or the intramolecular vibrations of the chromophores of mostly high-frequency modes. The intermolecular vibrational modes and the environmental fluctuations are generally characterized by a continuous bath spectral density. Many studies have suggested that a dissipative environment can be conducive to efficient quantum transport in a photosynthetic antenna complex,[23–28] e.g., by modulating energy transfer pathways to the reaction centre in favor of effective ones. The intramolecular high-frequency modes are often explicitly included as part of the primary system for strongly coupled modes in a vibronic model, which has been shown to be crucial to accurately predict the system dynamics such as coherences and relaxation rates that match the experimental results.[1,29,30]

While there is a general agreement that a dissipative environment can assist efficient energy transport in light-harvesting complexes, there is still some debate about the role of vibronic resonance between vibrational energy of the intramolecular nuclear mode and excitation-energy difference. It has been reported that vibronic resonance may be the key in enhancing electronic relaxation rate in cyanobacterial light-harvesting proteins[29] and that coupling to quantized vibrations that are quasi-resonant with transition energies can sustain coherent dynamics, which leads to fast and effective energy distribution in a preferential manner in cryptophyte algae.[22] O'Reilly and Olaya-Castro[15] suggested that non-classical features of the molecular vibration quasi-resonant with the excitonic energy splitting can drive efficient exciton population transfer in photosynthetic antennae systems. On the other hand, Kramer and Kreisbeck[31] reported that additional narrow peaks resonant with the energy

difference between the electronic eigenstates in the spectral density, which is represented by a superposition of shifted Drude-Lorentz peaks, do not lead to efficient transport in the FMO (Fenna-Matthews-Olson) complex. The role of vibronic resonance in coherent exciton dynamics has been also reported. A number of studies suggest that vibronic resonance can enhance coherences in light-harvesting complexes.[3,4,16,18,20–22] For instance, Chenu et al.[21] reported that resonance between the vibrational level and the electronic transition energy is required for the enhancement of vibronic and ground-state vibrational coherences in 2D spectra of a biological heterodimer. Other study suggests that it is the continuous part of the spectral density toward zero frequency that is crucial in determining long-lived coherence in the FMO complex and that additional peaks in the spectral density have only a small influence.[2]

Another issue concerning the role of vibronic resonance is how robust or sensitive vibronic enhancement is to environmental fluctuations, the strength of exciton-phonon interaction, and, in general, the details of the Hamiltonian. Lim et al.[4] suggested that vibronic resonance alone is not sufficient to lead to prolonged beating signals in an artificial molecular light harvester and that adequately low electronic decoherence rate determined by the interaction between system and bath is required to achieve vibronic enhancement. Fujihashi et al.[32] found that environmental fluctuations strongly suppress vibronic enhancement of electronic energy transfer both at cryogenic and physiological temperatures and that the long-lasting beating behavior in the 2D spectra disappears at physiological temperature using a coupled heterodimer representing BChls 3 and 4 in the FMO protein. In their studies it was assumed that electronic-vibrational coupling is weak (Huang-Rhys factor $S$=0.025) and that the modulation of the electronic coupling by the environment and nuclear DOFs is negligible and therefore only the fluctuation of the electronic energy was considered. Monahan et al.[33] explored the influence of $S$ on the oscillatory features in 2D spectra of a heterodimer of photosynthetic complexes, while constraining the total reorganization energy constant, and found greater long-lived inter-site coherences with increasing $S$ at 77 K, which vanishes at physiological temperatures due to environmental fluctuations. Sato and Doolittle[34] investigated the influence of intramolecular vibrations on coherences and population dynamics of BChl-protein dimer and found that larger $S$ leads to larger amplitude of coherences and higher energy transport efficiency and that higher reorganization energy yields higher transfer efficiencies. On the other hand, Plenio et al.[18] found most pronounced and long-lived

coherences in the excited state contribution for the intermediate Huang-Rhys factor of 0.02, while the amplitude of oscillations in the ground state contribution increases with the $S$. All these studies suggest that both factors, strength of intramolecular vibronic interaction and intermolecular/environmental system-bath interaction may play a role in vibronic enhancement and therefore their interplay needs to be taken into account.

In the studies above the environmental and nuclear DOFs are typically assumed to modulate the excitation energy and the fluctuation of the excitonic coupling is considered negligible. However, it has been recently reported that the fluctuation of the excitonic coupling can be as large as the average coupling itself in molecular aggregates.[35] For light-harvesting complexes, such as FMO complex, the widths of the distributions of the BChl couplings are roughly proportional to the absolute value of the couplings (e.g., several meV width for large coupling of $\sim$10 meV and less than 1 meV width for weaker coupling)[36] and the coupling fluctuation is smaller than the site energy fluctuation approximately by one order of magnitude.[37] It seems that the importance of the excitonic-coupling fluctuation is stronger for chromophores in close vicinity (as found in Light-Harvesting 2 (LH2) complex),[38] possibly because of the greater role of short-range interactions.

Herein we investigate vibronic enhancement of excitation energy transport with the fluctuations of the excitation energy *and* excitonic coupling taken into account by local (intramolecular/ diagonal) exciton-phonon interaction and non-local (intermolecular/ off-diagonal) exciton-phonon interaction, respectively. Here high-frequency vibrational modes strongly coupled to the electronic DOF are explicitly incorporated into the system Hamiltonian. The specific issues to be explored are three-fold: (i) the interplay between local and non-local exciton-phonon coupling in determining vibronic enhancement, (ii) the effect of field-induced initial-state generation and (iii) the role of multiple high-frequency modes with strong exciton-phonon coupling. Non-local exciton-phonon interaction, which is related to the fluctuation of the excitonic coupling, has been so far largely ignored and our work suggests that it plays more important role than previously thought in determining vibronic enhancement of excitation energy transport. In this work we also explore how the effect of initial state preparation is influenced by local and non-local exciton-phonon interaction. In many theoretical studies the initial state is often prepared by assuming instantaneous generation of localized exciton. However, this assumption does not exactly reflect the experiment, where the initial excitation is driven by a laser pulse. Explicitly accounting for system-field

interaction allows a description of system dynamics closer to the experimental condition.[39,40] Finally, we test the validity of employing a single effective vibrational mode. Schulze and Kühn[41] recently demonstrated using multi-layer multi-configuration time-dependent Hartree (ML-MCTDH) method that a large number of vibrational modes are excited in the FMO complex and therefore a single-effective-mode representation may be a rather strong approximation. Without exploring these features, any model would be at risk of giving the wrong *qualitative* results.

The combination of these effects is well suited to be explored by the surrogate Hamiltonian method,[42–45] which we have recently expressed in the vibronic basis.[46] This method, which was originally developed by Baer and Kosloff,[42] provides a means to study quantum dynamics of open systems without assuming either weak system-bath interaction or Markov approximation. Indeed in exciton transfer in light-harvesting complexes, the excitonic coupling is in the intermediate regime (comparable to the exciton-phonon interaction) and the timescale of bath relaxation cannot be assumed to be infinitely fast as compared to that of electronic dynamics.[40] The basic idea of the surrogate Hamiltonian method is to construct a finite system-bath Hamiltonian using the representative bath modes that span the typical energy range of the system, which can reproduce the true system dynamics in the limit of an infinite number of bath modes,[42,43] for a short-time system dynamics (before recurrence occurs due to the truncation of an infinite number of bath modes).

This paper is organized as follows. In section II we provide a brief description of the surrogate Hamiltonian method in a vibronic basis for a vibronically coupled molecular aggregate interacting with an external laser field. We discuss the results with a single effective mode in section III A and the effect of multi-mode coupling in section III B. Lastly we present a brief summary and outlook in section IV.

## II. METHOD

The total Hamiltonian can be described as the sum of the system, system-field interaction, bath, and system-bath interaction Hamiltonian terms

$$\hat{H} = \hat{H}_{\mathrm{S}} + \hat{H}_{\mathrm{SF}} + \hat{H}_{\mathrm{B}} + \hat{H}_{\mathrm{SB}}, \tag{1}$$

which will be defined in the following subsections.

### A. The primary system and the system-field interaction

The primary system Hamiltonian in a site basis, with effective vibrational modes included explicitly, can be written as[46]

$$\hat{H}_{\mathrm{S}} = \sum_{i,\boldsymbol{v}} \big(E_i + \hbar\boldsymbol{\omega}\cdot\boldsymbol{v}\big)|i,\boldsymbol{v}\rangle\langle i,\boldsymbol{v}| + \sum_{i,j\neq i}\sum_{\boldsymbol{v},\boldsymbol{w}} \tau_{ij} V^{i,j}_{\boldsymbol{v},\boldsymbol{w}} |i,\boldsymbol{v}\rangle\langle j,\boldsymbol{w}|, \tag{2}$$

where $|i,\boldsymbol{v}\rangle = |i; v_1 \cdots v_m \cdots\rangle$ denotes the vibronic state, where a monomer $i$ is in its electronic excited state and the rest is in their electronic ground state (we consider, when needed, a ground state with $i$=0); $E_i$ is the electronic site (excitation) energy localized on molecule $i$ with zero-point energy included; $\boldsymbol{\omega}$ and $\boldsymbol{v}$ are the vectors of vibrational frequency and vibrational quantum number, respectively, of vibronic state $|i,\boldsymbol{v}\rangle$; and $\tau_{ij}$ is the excitonic coupling between states $i$ and $j$. Here we consider one electronic excited state per molecule (and therefore the index $i$ can denote both electronic state and monomer) and each monomer can be coupled to any number of vibrational modes. All vibrations are assumed to be localized on a molecule. Here (multidimensional) Franck-Condon factor $V^{i,j}_{\boldsymbol{v},\boldsymbol{w}}$ can be written as

$$V^{i,j}_{\boldsymbol{v},\boldsymbol{w}} = \prod_m \mathcal{S}^{i,j}_{v_m,w_m}, \tag{3}$$

where $\mathcal{S}^{i,j}_{v_m,w_m}$ is the vibrational overlap integral for the vibrational mode $m$ associated with molecule $i$ or $j$ and determined by the Huang-Rhys factor $S^{i,j}_m$ and vibrational quantum number $v_m$ and $w_m$.[47] (Note that the Huang-Rhys factor $S^{i,j}_m$ is zero if $m$ is not localized on either $i$ or $j$.)

The interaction of the primary system with an external laser field that drives the excitation of the system can be written in the electric dipole approximation as

$$\hat{H}_{\mathrm{SF}} = -\hat{\mu} E_{\mathrm{ext}}(t), \tag{4}$$

where $E_{\mathrm{ext}}(t)$ describes the time-dependent electric field and $\hat{\mu}$ is the electronic transition dipole moment operator. (We assume that the transition dipole moment is constant in time and neglect the effect of different orientations of the transition dipole moment and the electric field.) Here the electric field is described as a Gaussian-shape pulse, given by[43,48]

$$E_{\mathrm{ext}}(t) = E_0 \exp\Big(-\frac{(t-t_0)^2}{2\sigma_p^2}\Big)\cos(\Omega_p t) = E_0 \exp\Big(-4\ln 2\frac{(t-t_0)^2}{\tau_p^2}\Big)\cos(\Omega_p t), \tag{5}$$

where $E_0, t_0, \sigma_p, \tau_p$ and $\Omega_p$ indicate the field intensity, pulse center, temporal pulse width, FWHM (full pulse width at half maximum), and carrier frequency, respectively. When the interaction with an external field is considered, we assume that the system is initially in the electronic ground state. In the vibronic basis the transition dipole moment operator $\hat{\mu}$ can be written as

$$\hat{\mu} = \sum_{i,\boldsymbol{v}} \mu_{eg}^{i,\boldsymbol{v}} |i, \boldsymbol{v}\rangle\langle 0, \boldsymbol{v}_0| + \text{h.c}, \tag{6}$$

where $|0, \boldsymbol{v}_0\rangle = |0; v_1^{(0)} \cdots v_m^{(0)} \cdots\rangle$ denotes an electronic ground state, where all molecular subunits are electronically unexcited, and $\mu_{eg}^{i,\boldsymbol{v}}$ is given by

$$\mu_{eg}^{i,\boldsymbol{v}} = \mu_{eg}^{(i)} \prod_m \mathcal{S}^{0,i}_{v_m^{(0)},v_m}, \tag{7}$$

with $\mu_{eg}^{(i)}$ being the electronic transition dipole moment of monomer $i$ from the ground state.

### B. Description of bath and system-bath interaction in the surrogate Hamiltonian approach

Surrogate Hamiltonian approach employs a spin bath model, where bath is described by non-interacting two-level systems,[42,44,45]

$$\hat{H}_{\text{B}} = \sum_k \varepsilon_k \hat{\sigma}_k^\dagger \hat{\sigma}_k, \tag{8}$$

where $\hat{\sigma}_k^\dagger/\hat{\sigma}_k$ is the creation/annihilation operator of the spin bath mode $k$ with energy $\varepsilon_k$. The spin bath, which can be considered as a low-temperature approximation of the harmonic oscillator,[42] provides an efficient way to propagate the wavefunction of the total Hamiltonian by employing a bit-ordered spinor without much deviation of the system dynamics as compared to using a harmonic bath.[45] There are in principle $2^M$ bath states for the spin bath with $M$ bath modes. However, the number of simultaneous excitations $N_{\text{exc}}$ can be restricted when the system-bath coupling is weak,[42,43,45,48] for which the number of bath states is reduced to $\sum_{k=0}^{N_{\text{exc}}} \binom{M}{k}$, where $\binom{M}{k} = \frac{M!}{k!(M-k)!}$ denotes the binomial coefficients.

In this work we do not consider pure dephasing process where decoherence occurs without the energy exchange between the system and bath. Therefore, the system-bath interaction Hamiltonian here describes the energy relaxation process, where the total energy of the system and bath remains constant. We note in passing that some decoherence is still present

in this process although we do not analyze it. The system-bath interaction Hamiltonian can be easily extended to include pure dephasing process if one is interested.[43] The system-bath Hamiltonian can be written as the sum of two interaction terms, each representing local ($\hat{H}^{(1)}_{\mathrm{SB}}$) and non-local ($\hat{H}^{(2)}_{\mathrm{SB}}$) interaction. (Description of system-bath interaction is provided in more detail in ref.[46]) In the local system-bath interaction Hamiltonian transitions involving only one vibrational quantum on the same molecular unit are allowed:

$$\hat{H}^{(1)}_{\mathrm{SB}} = \sum_{i,\boldsymbol{v}} \sum_{m} \Big[ \sqrt{v_m+1} \big| i; v_1, \cdots, v_m, \cdots \big\rangle \big\langle i; v_1, \cdots, v_m+1, \cdots \big| + \sqrt{v_m} \big| i; v_1, \cdots, v_m, \cdots \big\rangle \big\langle i; v_1, \cdots, v_m-1, \cdots \big| \Big] \sum_k c_k \big( \hat{\sigma}^{\dagger}_{mk} + \hat{\sigma}_{mk} \big). \quad (9)$$

Eq. 9 allows each bath mode to interact selectively with a limited number of vibronic states in its vicinity, as indicated by the site index $m$ in $\hat{\sigma}^{\dagger}_{mk}/\hat{\sigma}_{mk}$. The strength of the system-bath interaction is represented by the parameter $c_k$, which is set to be uniform regardless of the bath mode, i.e., $c_k = c$, in this work. We employ a discrete bath spectral density to describe local interaction, where bath mode energies are narrowly distributed around vibrational energy $\hbar\omega$ of the primary system. (Note that in the case of multi-mode coupling bath mode energies are centered around each intramolecular vibrational mode energy.)

The non-local system-bath interaction is associated with the transition occurring between different electronic states. This off-diagonal system-bath interaction term represents the fluctuation of the excitonic coupling, which has been largely neglected in other studies. The strength of the system-bath interaction is modulated by the nuclear modes that promote electronic transitions (Herzberg-Teller mechanism),[49–52] and therefore weighted by Franck-Condon factor between vibronic states associated with the transition:

$$\hat{H}^{(2)}_{\mathrm{SB}} = \sum_{i,\boldsymbol{v}} \sum_{j \neq i, \boldsymbol{w}} V^{i,j}_{\boldsymbol{v},\boldsymbol{w}} |i, \boldsymbol{v}\rangle\langle j, \boldsymbol{w}| \sum_k d_{k,ij} \big( \hat{\sigma}^{\dagger}_{ik} + \hat{\sigma}_{ik} + \hat{\sigma}^{\dagger}_{jk} + \hat{\sigma}_{jk} \big). \quad (10)$$

Here $d_{k,ij}$ represents the strength of system-bath interaction and could in principle depend on the molecular sites $(i, j)$. In this work we set $d_{k,ij} = d_k$. In surrogate Hamiltonian method $d_k$ is given by $d_k = \sqrt{\frac{J(\varepsilon_k)}{\rho(\varepsilon_k)}}$,[42–44] where $J(\varepsilon)$ and $\rho(\varepsilon)$ denote bath spectral density and bath density of modes, respectively. In this work we employ the Drude-Lorentz spectral density,[53,54] $J(\varepsilon) = 2\lambda\varepsilon\varepsilon_c/(\varepsilon^2 + \varepsilon_c^2)$, where $\lambda$ represents the strength of non-local exciton-phonon coupling, which can be related to the fluctuation of excitonic coupling, and $\varepsilon_c^{-1}$ is the characteristic time scale of the bath correlation function.

The main results of this manuscript includes the effect of the $\hat{H}^{(1)}_{\rm SB}$ and $\hat{H}^{(2)}_{\rm SB}$ components of the system-bath Hamiltonian. However, in the most general case one also has to include the effect of environmental fluctuations of the excitation energy. In the appendix we introduce local (diagonal) system-bath interaction Hamiltonian $\hat{H}^{(3)}_{\rm SB}$ to study this effect and report selected results. It should be noted that the diagonal exciton-phonon coupling has two contributions, i.e., one from high-frequency mode that is incorporated in the system Hamiltonian through the choice of a vibronic basis and the other from low-frequency modes that could be incorporated via the $\hat{H}^{(3)}_{\rm SB}$ component. However, the latter contribution is known to be much smaller: the reorganization energy, $E_r = \frac{1}{\pi}\int d\omega \frac{J(\omega)}{\omega}$, of the FMO complex[55] contributed from high-frequency ($\omega > 150$ cm$^{-1}$) and low-frequency mode ($\omega \leq 150$ cm$^{-1}$) is roughly 142 and 25 cm$^{-1}$, respectively.[70] For this reason it is useful to neglect the low-frequency diagonal exciton-phonon coupling in the first instance. For completeness the effect of its inclusion is given in the appendix.

We set the bath temperature to zero and therefore no bath mode is initially excited. The system-bath interaction leads to energy relaxation of the system to bath and, as a result, bath modes become excited from the ground state. It should be noted that exciton dynamics of the light-harvesting complexes can be influenced by the temperature.[24,32,33,56] Energy transfer efficiency in the FMO complex has been studied as a function of temperature using different quantum dynamics methods[24,56] and an optimal temperature with maximal efficiency has been reported.[56] The surrogate Hamiltonian method is able to describe finite temperature effect by initializing the population of the bath states to values compatible with a given temperature and repeating the simulation for an ensemble of initial conditions.[44] In this work, however, being interested in the vibronic resonance effect, we set the bath temperature to zero by setting all spin states to their ground states at $t$=0.

We assume that system and bath states are not entangled at $t$=0 and therefore initial wavefunction for the total system is given by $|\psi(0)\rangle = |\psi_{\rm S}(0)\rangle \otimes |\psi_{\rm B}(0)\rangle$. Here the primary system is in the electronic and vibrational ground state at $t$=0. Once $\psi(0)$ is determined, the time evolution of the wavefunction is obtained by $|\psi(t)\rangle = e^{-i\hat{H}t/\hbar}|\psi(0)\rangle$, which is carried out by expanding the time evolution operator by a series of Chebychev polynomials.[57–59] Then, the time evolution of the system observables can be evaluated using the reduced density

operator

$$\hat{\rho}_{\mathrm{S}}(t) = \mathrm{Tr}_{\mathrm{B}}\{\hat{\rho}(t)\} = \sum_{b} \langle b|\psi(t)\rangle\langle\psi(t)|b\rangle, \tag{11}$$

where $|b\rangle$ is the bath eigenstate and $\mathrm{Tr}_{\mathrm{B}}\{\ \}$ denotes a partial trace over the bath states.

### C. Parameters

In this work we focus on the interplay between local and non-local exciton-phonon coupling. The local exciton-phonon coupling is quantified by the Huang-Rhys factor $S$, it is associated with high-frequency intramolecular modes and it is part of our system Hamiltonian $H_{\mathrm{S}}$. The non-local exciton-phonon coupling is quantified by the coupling strength $\lambda$ in $H_{\mathrm{SB}}^{(2)}$ and it is associated with environmental (intermolecular and low-frequency) motions. We do not explore instead the role of the vibrational relaxation strength (parameter $c$ in $H_{\mathrm{SB}}^{(1)}$) because this term is outside the scope of this work and likely to be similar for most systems.

We consider a heterodimer system that represents two cyanobacterial light-harvesting proteins, allophycocyanin (APC) and C-phycocyanin (CPC), which were extensively studied both theoretically and experimentally.[29,60–63] Using a vibronic exciton model, Womick and Moran suggested that vibronic resonance between the hydrogen out-of-plane mode and the electronic energy gap is responsible for much faster relaxation rate observed for APC despite the almost identical structures of pigment dimers ($\alpha$84 and $\beta$84) in APC and CPC.[29] (We denote $\alpha$84 and $\beta$84 as 1 and 2 for the remainder of this paper.) In their study the rate constants corresponding to a transition from one excitonic state to another were obtained using a modified Redfield theory. In this work we employ the same parameters that are used in ref.[29] except that we vary both local exciton-phonon coupling strength (Huang-Rhys factor $S$) and non-local exciton-phonon coupling strength $\lambda$ in order to see how vibronic enhancement is influenced by the interplay between these two. We can estimate $\lambda$ from the fluctuation of excitonic coupling in the classical high-temperature limit, $\sigma_\tau \sim \sqrt{\lambda\ k_{\mathrm{B}}T}$. The range of $\lambda$ considered in this work (5-300 cm$^{-1}$) corresponds to $\sigma_\tau$=0.2$\tau$-1.7$\tau$ in agreement with the fluctuation of the excitonic coupling reported in molecular crystals.[35,64] The parameter values used here are as follows: $\Delta E_{\mathrm{APC}}$=760 cm$^{-1}$ (here $\Delta E = E_2 - E_1$, where $E_1$ and $E_2$ denote the non-interacting excitation energy of the monomer 1 and 2 from the ground state - see Figure 1), $\Delta E_{\mathrm{CPC}}$ = 350 cm$^{-1}$, $\tau$ = −150 cm$^{-1}$, $\varepsilon_c^{-1}$ = 238 fs. We

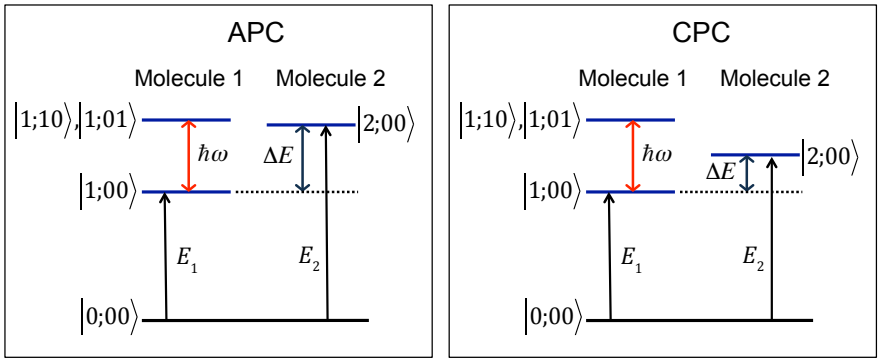


FIG. 1: Schematic of the energy levels of the dimer in APC and CPC.

impose an energy threshold to limit the number of vibrational states included in the system Hamiltonian in such a way that total four excited states are included in the primary system in the case of single effective vibrational mode ($|1;00\rangle, |1;10\rangle, |1;01\rangle, |2;00\rangle$).

The electric field is described using the parameter values of $t_0$=50 fs and $\tau_p$=50 fs. The carrier frequency $\Omega_p$ is set to the excitation energy of site 2. The electronic transition dipole moment, which is assumed be the same for both monomers, and the field intensity $E_0$ are chosen in such a way that about a few tenth of population is transferred to site 1 after initial excitation (here $E_0\mu_{eg}^{(1)} = E_0\mu_{eg}^{(2)}$ was set to 0.02 eV=161 cm$^{-1}$).

The surrogate Hamiltonian method allows the propagation of the wavefunction for a finite time beyond which the finite size of the bath causes unphysical recurrences.[42] For the simulation time considered here recurrence does not occur and the results are not affected by the increase in the bath size. For the local system-bath interaction the system-bath coupling strength is set to $c$=8 cm$^{-1}$ and bath spectral density is constructed to have uniform energy spacing $\delta\varepsilon_k$=16 cm$^{-1}$. The number of bath modes used for the local and non-local system-bath interaction is 15 and 18, respectively, and the number of simultaneous excitations is restricted to $N_{\text{exc}}$=2. The bath parameters, such as $c$, $\delta\varepsilon_k$, $N_{\text{exc}}$, and the number of bath modes, have been tested for convergence.

## III. RESULTS

### A. Single effective vibrational mode

In this section we describe exciton dynamics when a single effective vibrational mode is incorporated into the system Hamiltonian. More specifically, we first present how vibronic resonance influences the efficiency of site population transfer by considering different values of excitation energy splitting of non-interacting monomers. Next we describe how vibronic enhancement induced by resonance condition is affected by the interplay between local and non-local exciton-phonon coupling strength. Lastly we present the effect of field-driven excitation on population dynamics in comparison with instantaneous generation of localized exciton.

Here intramolecular vibrational mode frequency $\omega$ is set to 800 cm$^{-1}$, which corresponds to hydrogen out-of-plane wagging vibration as in ref.[29] Since we consider a dimer system, the Franck-Condon factor $V^{i,j}_{\boldsymbol{v},\boldsymbol{w}}$ $(i,j \neq 0)$ can be parameterized by a single Huang-Rhys factor $S$; $V^{1,2}_{(10),(00)} = V^{1,2}_{(01),(00)} = \mathcal{S}^{1,2}_{1,0}\ \mathcal{S}^{1,2}_{0,0} = \sqrt{S}e^{-S}$ and $V^{1,2}_{(00),(00)} = \mathcal{S}^{1,2}_{0,0}\ \mathcal{S}^{1,2}_{0,0} = e^{-S}$.

#### *1. Resonance-driven vibronic enhancement*

Figure 2a shows the population of site 1 for APC and CPC obtained with Huang-Rhys factor $S$=0.125 and non-local exciton-phonon coupling strength $\lambda$=100 cm$^{-1}$, where dashed line indicates the population of site 2 of APC ($S$=0.125 is taken from ref.[29]). Here the population of site $i$ is obtained by $P_i(t) = \sum_{\boldsymbol{v}} \langle i, \boldsymbol{v}|\hat{\rho}_{\mathrm{S}}(t)|i, \boldsymbol{v}\rangle$. It demonstrates that more population is transferred to site 1 in APC as compared to CPC despite the much smaller excitation energy gap in CPC (350 vs. 760 cm$^{-1}$). More efficient population transfer of APC arises from close proximity of the intramolecular vibrational mode (800 cm$^{-1}$) to the excitation-energy gap (760 cm$^{-1}$) for APC.

In order to see if the resonance of energy levels between vibrational mode and transition energy is responsible for more efficient population transfer in APC, we obtain the population dynamics as a function of excitation energy gap, $\Delta E$, while keeping the vibrational mode energy the same ($\omega$=800 cm$^{-1}$). As a quantitative measure of the efficiency of site population transfer, we compute the time-averaged population of site 1 over the time window $t_w$, defined as $\eta \equiv (1/t_w)\int_0^{t_w} dt P_1(t)$.[15,65,66] (Note that exciton is often delocalized on more than one site

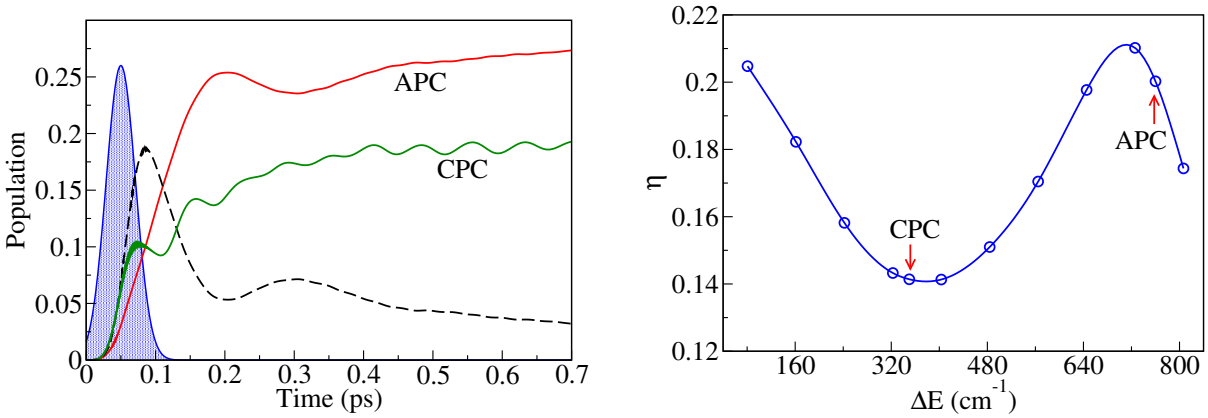


(a) (b)

FIG. 2: (a) Time evolution of population of site 1 for APC and CPC with $\lambda$=100 cm$^{-1}$ and $S$=0.125. Here dashed line indicates population of site 2 for APC and shaded area indicates the laser pulse intensity in arbitrary unit. (b) Efficiency $\eta$ of site population transfer as a function of excitation energy gap for $t_w$=0.5 ps, $\lambda$=100 cm$^{-1}$ and $S$=0.125.

and therefore we refer to $\eta$ as an efficiency of site population transfer rather than exciton transfer efficiency.) Figure 2b shows the efficiency $\eta$ as a function of $\Delta E$ for $S$=0.125 and $\lambda$=100 cm$^{-1}$. The efficiency is largest when the $\Delta E$ becomes very small or when the energy splitting between excitonic states (eigenstates), $\Delta\varepsilon = \sqrt{(\Delta E)^2 + 4\tau^2}$, becomes close to the vibrational energy $\hbar\omega$. The ratio of $\eta$ at its maximum to that at its minimum is not very large (=1.5), suggesting that vibronic enhancement is rather weak for the parameter values used here for local and non-local exciton-phonon coupling. We note in passing that our result is not necessarily at odds with the earlier report,[31] where adding specific narrow modes to the continuous bath spectral density of the FMO complex has only a minor impact on the energy transfer efficiency, in that vibronic enhancement obtained here for a given exciton-phonon coupling is rather weak and it becomes even smaller as the non-local exciton-phonon coupling increases as we describe in section III A 2. In addition, resonant vibrational mode is explicitly incorporated in the system Hamiltonian in this work rather than represented by additional peaks in the continuous spectral density.

*2. Impact of exciton-phonon coupling strength on vibronic enhancement*

We first consider the influence of local (intramolecular) exciton-phonon interaction on vibronic enhancement. Figure 3a shows the efficiency $\eta$ (solid line) as a function of Huang-Rhys factor $S$, ranging from 0.025 to 1, where $\lambda$ is set to 100 cm$^{-1}$. (Note that $\eta$ is evaluated as a function of $S$ for different values of $\lambda$ as well, varying from 5 to 300 cm$^{-1}$.) For APC with transition energy quasi-resonant with vibrational energy, the efficiency increases as the $S$ increases, reaches maximum at $S$ $\sim$0.5, and then decreases with $S$, whereas $\eta$ shows a monotonic decay with $S$ for CPC with off-resonant transition energy. This can be easily understood from the expression of Franck-Condon factor in terms of $S$, $V^{1,2}_{(10),(00)} = \sqrt{S}e^{-S}$ and $V^{1,2}_{(00),(00)} = e^{-S}$. In other words, vibrational coupling between the vibrational excited state of site 1 and ground state of site 2, $V^{1,2}_{(10),(00)}$ and $V^{1,2}_{(01),(00)}$, increases with $S$, reaches maximum at $S$=0.5 and then decreases slowly with $S$, whereas vibrational coupling between the ground states of site 1 and 2, $V^{1,2}_{(00),(00)}$, decreases exponentially with $S$. For APC the transition between the states $|1;10\rangle$ (and $|1;01\rangle$) and $|2;00\rangle$ is a dominant process due to the small energy gap between these two states and therefore the behavior of $\eta(S)$ is mostly determined by $V_{(1;10),(2;00)}$ (and $V_{(1;01),(2;00)}$). On the other hand, for CPC with transition energy significantly detuned from the vibrational energy, the population dynamics is mostly determined by the transition between the $|1;00\rangle$ and $|2;00\rangle$ states and therefore $\eta$ decreases with $S$. We note in passing that for APC the value of $S$ with largest $\eta$ is slightly influenced by the $\lambda$ as well. For large $\lambda$, intermolecular relaxation from site 2 to the ground state of site 1 becomes more dominant and therefore $\eta$ becomes largest at smaller value of $S$ than 0.5 due to the decrease of $V^{1,2}_{(00),(00)}$ with $S$. (Note that non-local system-bath interaction depends on the Franck-Condon factor as well - see eq. 10). The ratio of efficiency between APC and CPC, $\eta_{\mathrm{APC}}/\eta_{\mathrm{CPC}}$, is also plotted in dashed line in Figure 3a. It illustrates that population transfer is more efficient for APC for all values of $S$ considered here (even as small as 0.025) due to the close proximity of the transition energy to the vibrational energy despite the larger transition energy. As expected, $\eta_{\mathrm{APC}}/\eta_{\mathrm{CPC}}$ increases with $S$.

We next consider how vibronic enhancement is influenced by the non-local exciton-phonon interaction. To this end, we evaluate the efficiency $\eta$ as a function of $\lambda$ for a given value of $S$. Figure 3b shows how $\eta$ varies with $\lambda$ for $S$=0.125. For APC $\eta$ exhibits a non-monotonic behavior with $\lambda$, reaching a maximum at $\lambda$=20 cm$^{-1}$. As the $\lambda$ increases further,

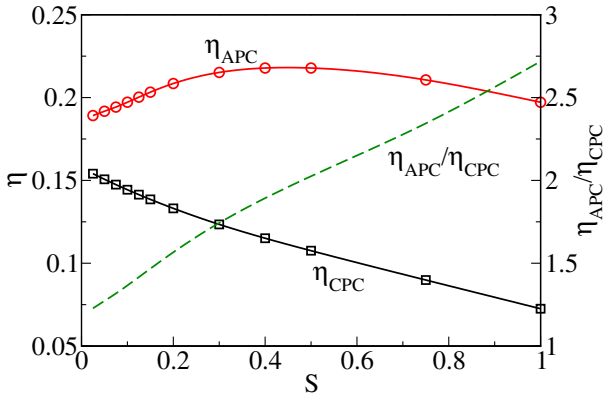


(a)

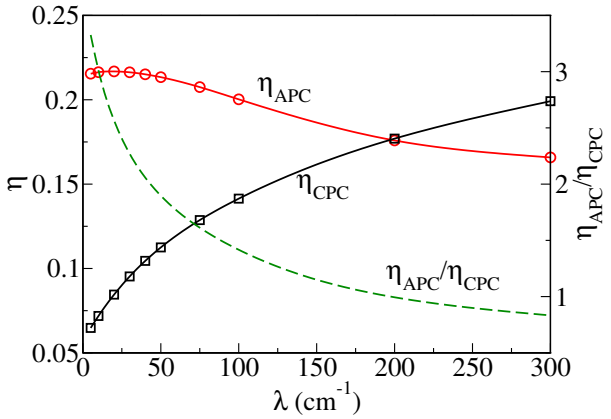


(b)

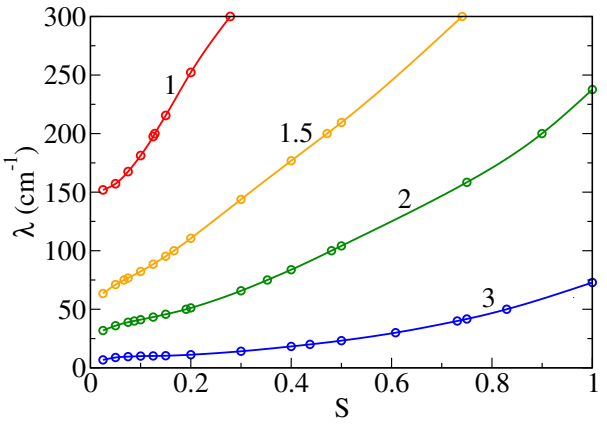


(c)

FIG. 3: Efficiency $\eta$ of site population transfer (solid lines) in APC and CPC and efficiency ratio $\eta_{\rm APC}/\eta_{\rm CPC}$ (dashed line) (a) as a function of $S$ with $\lambda$=100 cm$^{-1}$ and (b) as a function of $\lambda$ with $S$=0.125. (c) Contour plot of $\eta_{\rm APC}/\eta_{\rm CPC}$ as a function of $S$ and $\lambda$. Each contour line corresponds to $\eta_{\rm APC}/\eta_{\rm CPC}$=1, 1.5, 2, and 3. The vibronic enhancement in terms of efficiency ratio between APC and CPC becomes stronger as the $S$ increases and the $\lambda$ decreases.

vibronic enhancement is suppressed. This dependency of $\eta$ on $\lambda$ hints at the possibility of tuning vibronic enhancement by the interaction with a thermal environment. We note in passing that the trend of $\eta(\lambda)$ shown here can be sensitive to other parameters such as $\varepsilon_c$, $S$, etc. For the off-resonant case (CPC), the efficiency shows a monotonic increase with $\lambda$ since thermally activated transport is a dominant transport mechanism. As a result, the ratio of efficiency, $\eta_{\mathrm{APC}}/\eta_{\mathrm{CPC}}$, almost exponentially decays with $\lambda$, as indicated by the dashed line in Fig. 3b. Therefore, the effect of vibronic resonance on efficient site population transfer becomes negligible when system-bath interaction dominates the transport process. Our finding is in line with the results by Fujihashi et al.[32], where environmentally induced fluctuations and dissipation hinders the contribution of vibronic resonance to the efficient energy transfer in heterodimer pigment molecules in the FMO protein. It should be noted that in ref.[32] the protein environment induces fluctuations of the electronic energy, whereas non-local exciton-phonon coupling strength $\lambda$ in this work represents the modulation of the excitonic coupling.

To see how vibronic enhancement is determined by the interplay between these two types of exciton-phonon interaction, we plot contours as a function of $S$ and $\lambda$ in Figure 3c, where each line corresponds to $\eta_{\mathrm{APC}}/\eta_{\mathrm{CPC}}$=1, 1.5, 2, and 3. It shows that vibronic enhancement in terms of efficiency ratio between APC and CPC becomes stronger as intramolecular exciton-phonon coupling strength $S$ increases and non-local intermolecular/environmental coupling strength $\lambda$ decreases. We find that therefore vibronic enhancement can be achieved even for a very small value of $S$ when $\lambda$ is small (e.g., for $\lambda$ <152 cm$^{-1}$ $\eta_{\mathrm{APC}}$ is larger than $\eta_{\mathrm{CPC}}$ for all considered values of $S$ here), whereas large $S$ is required to achieve higher efficiency in APC for large $\lambda$. It is also seen that vibronic enhancement becomes more sensitive to $\lambda$ for smaller $S$. Considering that Huang-Rhys factor is in general rather small for pigment molecules in photosynthetic complexes, our result suggests that how to control intermolecular and environmental coupling strength may be critical to maximize vibronic enhancement. It further indicates that for the plausible range of $\lambda$, which corresponds to the fluctuation of excitonic coupling below or similar to the average value ($\lambda \leq$100 cm$^{-1}$), the effect of vibronic enhancement is not dramatic (roughly by a factor of no more than 3).

*3. Effect of field-driven excitation*

Figure 4a shows the population of site 1 for $S$=0.125 and $\lambda$=100 cm$^{-1}$ when the initial state is prepared by the instantaneous generation of localized exciton on site 2 rather than a field-driven excitation. Overall trend of time evolution of population is similar for both field-free and field-driven excitation except that for the former population transfer to site 1 in CPC seems to occur faster and population exhibits high-frequency oscillatory behavior, which originates from the coherences between $|1;00\rangle$ and $|2;00\rangle$ states, whereas it is strongly suppressed for the latter (see Figure 2a).

The efficiency of population transfer is plotted as a function of $S$ for $\lambda$=100 cm$^{-1}$ and as a function of $\lambda$ for $S$=0.125 in Figure 4b and 4c, respectively. We note in passing that direct comparison of $\eta$ between different excitations cannot be made because initial population is very different depending on the initial-state preparation, i.e., site 2 is only partially populated after the laser field is turned on, whereas it is fully populated ($P_2(0)$=1) for instantaneous excitation. We find that the overall trend of efficiency $\eta$ as a function of $S$ and as a function of $\lambda$ is similar for both excitations, i.e., $\eta$ is largest at $S \sim$ 0.5-0.75 for APC but decays monotonically with $S$ for CPC and $\eta$ is largest at $\lambda$=20 cm$^{-1}$ for APC but increases monotonically with $\lambda$ for CPC. As a result, the ratio of efficiency, $\eta_{\mathrm{APC}}/\eta_{\mathrm{CPC}}$, as a function of $S$ and as a function of $\lambda$ shows a similar trend regardless of initial state preparation (see dashed line), although it is slightly smaller for instantaneous excitation due to faster relaxation in CPC. Despite differences in details we conclude that whether initial excitation is induced by the interaction with an external field or localized exciton state is instantaneously generated does not make qualitative differences in population dynamics, consistently with the simulation results obtained for the FMO complex by Schulze et al.[39]

## B. Two effective vibrational modes

Spectral densities of the FMO complex obtained using different computational methods[55,67,68] and difference fluorescence line narrowing ($\Delta$FLN) experiments[69] exhibit several intramolecular high-frequency modes with large amplitude. In this section we consider the case where there is more than one effective vibrational mode coupled to the electronic DOF and investigate its impact on vibronic enhancement. To this end we incorporate sec-

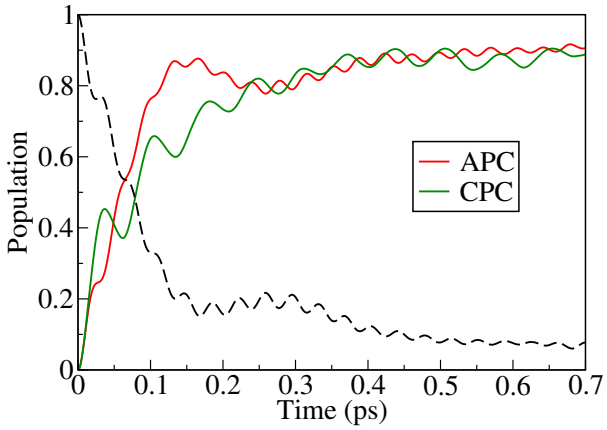


(a)

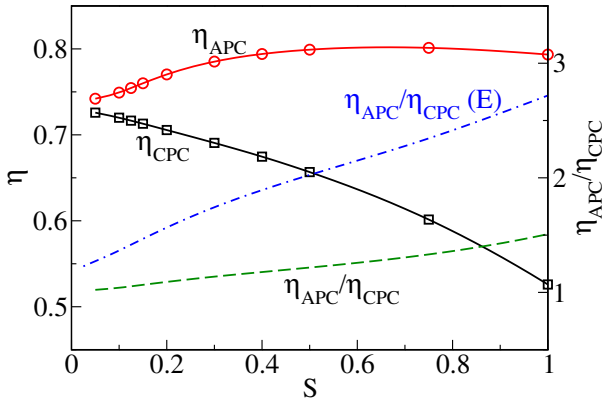


(b)

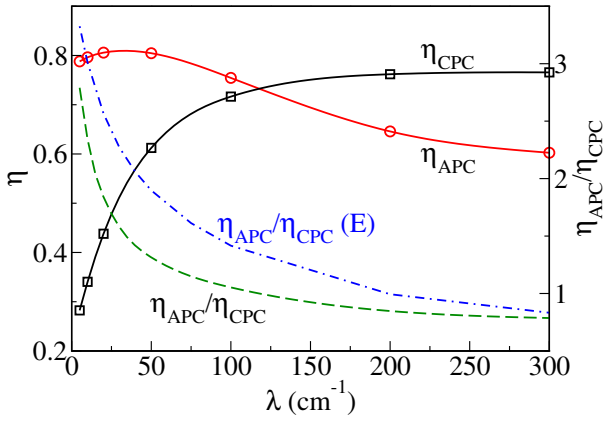


(c)

FIG. 4: (a) Population of site 1 for APC and CPC with $\lambda$=100 cm$^{-1}$ and $S$=0.125 when site 2 is instantaneously excited. (Dashed line indicates population of site 2 for APC.) (b) Transfer efficiency $\eta$ as a function of $S$ for $\lambda$=100 cm$^{-1}$ and (c) as a function of $\lambda$ for $S$=0.125. The efficiency ratio, $\eta_{\rm APC}/\eta_{\rm CPC}$, is plotted in dashed line. (Dot-dashed line indicates $\eta_{\rm APC}/\eta_{\rm CPC}$ when initial excitation is driven by a laser pulse.)

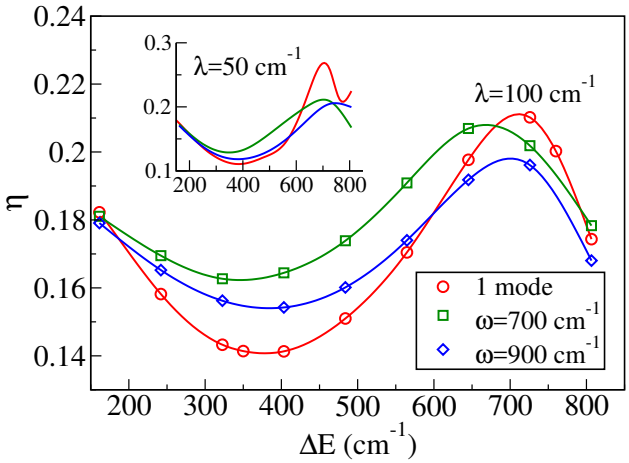


FIG. 5: Efficiency of site population transfer as a function of excitation energy splitting where two vibrational modes are coupled to the electronic state for two different frequencies (700 or 900 $\mathrm{cm}^{-1}$) as compared to single effective mode coupling. Here the frequency of the first vibrational mode and the total system reorganization energy remain constant in all cases and $\lambda$ is set to 100 $\mathrm{cm}^{-1}$ (inset shows the result for $\lambda$=50 $\mathrm{cm}^{-1}$).

ond vibrational mode ($\omega$=700 or 900 $\mathrm{cm}^{-1}$) in the system Hamiltonian, where the frequency of the first vibrational mode is kept the same as in section III A ($\omega$=800 $\mathrm{cm}^{-1}$). We also assume that two modes are coupled with equal strength, i.e., $S$ is the same for both modes, and total system reorganization energy, $\sum_{i=1,2} S_i \hbar\omega_i$, remains constant. The energy cutoff in the system Hamiltonian is imposed in such a way that monomer 1 is excited by up to one vibrational quantum of each mode and monomer 2 with higher excitation energy is in the vibrational ground state in all cases.

Figure 5 shows the efficiency as a function of excitation energy splitting with two high-frequency mode coupling, where the efficiency for a single effective mode coupling is also plotted for comparison. Similar trend of $\eta$ is found as a function of $\Delta E$, i.e., larger efficiency with small energy barrier or in the presence of vibronic resonance. However, we also find that overall the difference in efficiency between resonance and off-resonance case is reduced when two vibrational modes are coupled. In other words, modest vibronic enhancement observed for a single effective mode coupling becomes even smaller when more than one vibrational mode is coupled, which is likely to be the case in realistic systems.

## IV. CONCLUSIONS

In summary we presented how vibronic enhancement induced by quasi-resonant alignment of intramolecular vibrational energy with the excitation energy splitting is influenced by the interplay between local (intramolecular) and non-local exciton-phonon interaction using a heterodimer model, where initial excitation is driven by a time-dependent external field. Our calculation suggests that vibronic resonance leads to more efficient transfer of site population in the plausible range of local and non-local exciton-phonon coupling strength. We also find that vibronic enhancement driven by the resonance of intramolecular vibrational mode is sensitive to the strength of non-local exciton-phonon interaction and vanishes as it becomes (moderately) strong, of which threshold is determined by the strength of local exciton-phonon interaction (Huang-Rhys factor). Therefore, our results indicate that the interplay between intramolecular local vibronic coupling and intermolecular non-local exciton-phonon interaction needs to be taken into account in order to achieve efficient exciton transport in artificial light-harvesting complexes. Our work also brings new insight into the role of non-local exciton-phonon coupling, which represents the fluctuation of excitonic coupling, in exciton dynamics.

We found that simulation of field-driven excitation does not significantly alter the population dynamics in terms of the behavior of population transfer efficiency as a function of local and non-local exciton-phonon coupling strength when compared to the instantaneous excitation although detailed features of population dynamics may not be the same. In realistic systems it is likely that more than one effective vibrational mode is strongly coupled to the system. In this scenario, we find that the impact of vibronic resonance on population transfer becomes weaker regardless of whether environmental exciton-phonon interaction is described by local (diagonal) or non-local (off-diagonal) coupling, indicating that vibroinc resonance, in reality, may not be such a decisive factor to achieve higher efficiency in excitation energy transfer.

Our work can be extended in the future to combine our quantum dynamics methodology with first-principles calculation to obtain/employ parameters that can represent realistic systems more closely.

**ACKNOWLEDGMENTS**

This work was supported by ERC through Grant No. 615834.

**APPENDIX**

The system-bath Hamiltonian in section II B can be extended to include the fluctuation of the excitation energy due to the interaction with the environment, which can be described by diagonal exciton-phonon interaction term

$$\hat{H}_{\mathrm{SB}}^{(3)} = \sum_{i,\boldsymbol{v}} |i,\boldsymbol{v}\rangle\langle i,\boldsymbol{v}| \sum_{k} g_{k,i}\big(\hat{\sigma}_{ik}^{\dagger} + \hat{\sigma}_{ik}\big), \tag{12}$$

where $g_{k,i}$ represents the coupling strength of site $i$ to mode $k$. In this work $g_{k,i}$ is assumed to be independent of site $i$ ($g_{k,i} = g_k$) and given by $g_k = \sqrt{\frac{J(\varepsilon_k)}{\rho(\varepsilon_k)}}$, where $J(\varepsilon)$ is bath spectral density and $\rho(\varepsilon)$ is bath density of modes. We employ the Drude-Lorentz spectral density $J(\varepsilon) = 2\tilde{\lambda}\varepsilon\varepsilon_{\mathrm{c}}/(\varepsilon^2 + \varepsilon_{\mathrm{c}}^2)$, where $\tilde{\lambda}$ represents the strength of local (diagonal) exciton-phonon interaction and can be related to the fluctuation of the site energy.

To see the effect of local exciton-phonon interaction on vibronic enhancement, we obtain population dynamics with $\hat{H}_{\mathrm{SB}}^{(3)} \neq 0$ and $\hat{H}_{\mathrm{SB}}^{(2)} = 0$, where $\hat{H}_{\mathrm{SB}}^{(1)}$ and $\hat{H}_{\mathrm{SF}}$ are included using the same parameters employed in section III. In Figure 6 the efficiency $\eta$ of population transfer is plotted for $\tilde{\lambda}$=100 cm$^{-1}$ as a function of excitation energy splitting $\Delta E$, where two cases (a single effective vibrational mode coupling and two high-frequency mode coupling) are considered (inset shows the result for $\tilde{\lambda}$=50 cm$^{-1}$). The overall trend of $\eta(\Delta E)$ is similar to that of non-local exciton-phonon coupling, i.e., $\eta$ decreases as $\Delta E$ increases, reaches a minimum, and increases as the energy level alignment becomes closer to vibronic resonance. The difference in $\eta$ between resonant and off-resonant case is also reduced when two vibrational modes are coupled as compared to a single mode coupling for both $\tilde{\lambda}$=100 and 50 cm$^{-1}$. It is also seen that vibronic enhancement is suppressed as $\tilde{\lambda}$ increases from 50 to 100 cm$^{-1}$ for both single and two mode coupling.

We note that vibronic enhancement appears to be slightly stronger for local exciton-phonon coupling ($\hat{H}_{\mathrm{SB}}^{(3)}$) as compared to non-local exciton-phonon coupling ($\hat{H}_{\mathrm{SB}}^{(2)}$) for the same magnitude of exciton-phonon coupling strength ($\lambda = \tilde{\lambda}$). For instance, the difference between the largest and smallest efficiency for a single mode coupling with $\lambda = \tilde{\lambda}$=100

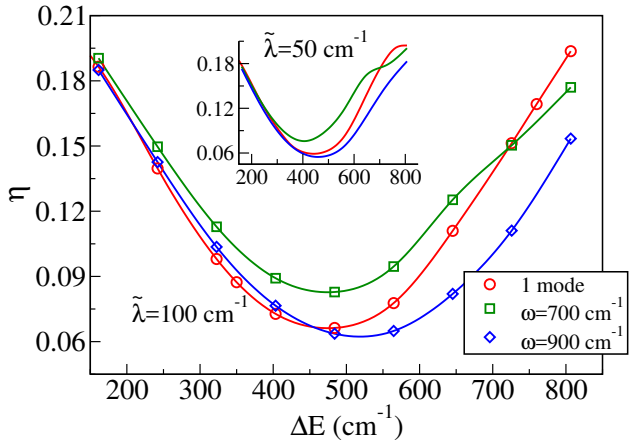


FIG. 6: Efficiency of site population transfer as a function of excitation energy splitting, where two high-frequency mode coupling is compared to a single effective mode coupling with $\hat{H}_{\rm SB}^{(3)} \neq 0$, $\hat{H}_{\rm SB}^{(2)} = 0$ and $\tilde{\lambda}$=100 cm$^{-1}$. (The rest of parameters are kept the same as section III B and inset shows the efficiency with $\tilde{\lambda}$=50 cm$^{-1}$.)

cm$^{-1}$ is 0.13 and 0.07 for local and non-local exciton-phonon coupling, respectively (the same trend is also found for two-mode coupling and different coupling strength ($\lambda = \tilde{\lambda}$=50 cm$^{-1}$)). It should be noted that, however, $\lambda$ and $\tilde{\lambda}$ have different meanings and therefore direct comparison between local and non-local exciton-phonon coupling cannot be made. To sum up, we reach a similar conclusion by employing either local or non-local coupling that vibronic enhancement becomes suppressed as the strength of exciton-phonon coupling and/or the number of strongly coupled high-frequency modes increases.

* mail to: myeong.lee@warwick.ac.uk

[1] N. Christensson, H. F. Kauffmann, T. Pullerits, and T. Mančal, J. Phys. Chem. B **116**, 7449 (2012).

[2] C. Kreisbeck and T. Kramer, J. Phys. Chem. Lett. **3**, 2828 (2012).

[3] A. W. Chin, J. Prior, R. Rosenbach, F. Caycedo-Soler, S. F. Huelga, and M. B. Plenio, Nature Phys. **9**, 113 (2013).

[4] J. Lim, D. Paleček, F. Caycedo-Soler, C. N. Lincoln, J. Prior, H. von Berlepsch, S. F. Huelga, M. B. Plenio, D. Zigmantas, and J. Hauer, Nature Commun. **6**, 7755 (2015).

[5] A. Halpin, P. J. M. Johnson, R. Tempelaar, R. S. Murphy, J. Knoester, T. L. C. Jansen, and R. J. D. Miller, Nature Chem. **6**, 196 (2014).

[6] E. Romero, R. Augulis, V. I. Novoderezhkin, M. Ferretti, J. Thieme, D. Zigmantas, and R. van Grondelle, Nature Phys. **10**, 676 (2014).

[7] F. D. Fuller, J. Pan, A. Gelzinis, V. Butkus, S. S. Senlik, D. E. Wilcox, C. F. Yocum, L. Valkunas, D. Abramavicius, and J. P. Ogilvie, Nature Chem. **6**, 706 (2014).

[8] S. M. Falke, C. A. Rozzi, D. Brida, M. Maiuri, M. Amato, E. Sommer, A. D. Sio, A. Rubio, G. Cerullo, E. Molinari, et al., Science **344**, 1001 (2014).

[9] H. Tamura, R. Martinazzo, M. Ruckenbauer, and I. Burghardt, J. Chem. Phys. **137**, 22A540 (2012).

[10] A. J. Musser, M. Liebel, C. Schnedermann, T. Wende, T. B. Kehoe, A. Rao, and P. Kukura, Nature Phys. **11**, 352 (2015).

[11] A. A. Bakulin, S. E. Morgan, T. B. Kehoe, M. W. B. Wilson, A. W. Chin, D. Zigmantas, D. Egorova, and A. Rao, Nature Chem. **8**, 16 (2015).

[12] S. Ito, T. Nagami, and M. Nakano, J. Phys. Chem. Lett. **6**, 4972 (2015).

[13] N. Renaud and F. C. Grozema, J. Phys. Chem. Lett. **6**, 360 (2015).

[14] Y. Song, S. N. Clafton, R. D. Pensack, T. W. Kee, and G. D. Scholes, Nature Commun. **5**, 4933 (2014).

[15] E. J. O'Reilly and A. Olaya-Castro, Nature Commun. **5**, 3012 (2014).

[16] V. Tiwari, W. K. Peters, and D. M. Jonas, Proc. Natl. Acad. Sci. USA **110**, 1203 (2013).

[17] M. Schröter, T. Pullerits, and O. Kühn, Ann. Phys. (Berlin) **527**, 536 (2015).

[18] M. B. Plenio, J. Almeida, and S. F. Huelga, J. Chem. Phys. **139**, 235102 (2013).

[19] M. Schröter, S. D. Ivanov, J. Schulze, S. P. Polyutov, Y. Yan, T. Pullerits, and O. Kühn, Phys. Rep. **567**, 1 (2015).

[20] F. Novelli, A. Nazir, G. H. Richards, A. Roozbeh, K. E. Wilk, P. M. G. Curmi, and J. A. Davis, J. Phys. Chem. Lett. **6**, 4573 (2015).

[21] A. Chenu, N. Christensson, H. F. Kauffmann, and T. Mančal, Sci. Rep. **3**, 02029 (2013).

[22] A. Kolli, E. J. O'Reilly, G. D. Scholes, and A. Olaya-Castro, J. Chem. Phys. **137**, 174109 (2012).

[23] A. Ishizaki and G. R. Fleming, Proc. Natl. Acad. Sci. USA **106**, 17255 (2009).

[24] M. Mohseni, P. Rebentrost, S. Lloyd, and A. Aspuru-Guzik, J. Chem. Phys. **129**, 174106 (2008).

[25] P. Rebentrost, M. Mohseni, I. Kassal, S. Lloyd, and A. Aspuru-Guzik, New J. Phys. **11**, 033003 (2009).

[26] M. B. Plenio and S. F. Huelga, New J. Phys. **10**, 113019 (2008).

[27] F. Caruso, A. W. Chin, A. Datta, S. F. Huelga, and M. B. Plenio, J. Chem. Phys. **131**, 105106 (2009).

[28] A. W. Chin, A. Datta, F. Caruso, S. F. Huelga, and M. B. Plenio, New J. Phys. **12**, 065002 (2010).

[29] J. M. Womick and A. M. Moran, J. Phys. Chem. B **115**, 1347 (2011).

[30] S. Polyutov, O. Kühn, and T. Pullerits, Chem. Phys. **394**, 21 (2012).

[31] T. Kramer and C. Kreisbeck, AIP Conf. Proc. **1575**, 111 (2014).

[32] Y. Fujihashi, G. R. Fleming, and A. Ishizaki, J. Chem. Phys. **142**, 212403 (2015).

[33] D. M. Monahan, L. Whaley-Mayda, A. Ishizaki, and G. R. Fleming, J. Chem. Phys. **143**, 065101 (2015).

[34] Y. Sato and B. Doolittle, J. Chem. Phys. **141**, 185102 (2014).

[35] J. Aragó and A. Troisi, Phys. Rev. Lett. **114**, 026402 (2015).

[36] C. Olbrich, T. L. C. Jansen, J. Liebers, M. Aghtar, J. Strümpfer, K. Schulten, J. Knoester, and U. Kleinekathöfer, J. Phys. Chem. B **115**, 8609 (2011).

[37] T. Renger, A. Klinger, F. Steinecker, M. S. am Busch, J. Numata, and F. Müh, J. Phys. Chem. B **116**, 14565 (2012).

[38] C. P. van der Vegte, J. D. Prajapati, U. Kleinekathöfer, J. Knoester, and T. L. C. Jansen, J. Phys. Chem. B **119**, 1302 (2015).

[39] J. Schulze, M. F. Shibl, M. J. Al-Marri, and O. Kühn, J. Chem. Phys. **144**, 185101 (2016).

[40] F. Fassioli, R. Dinshaw, P. C. Arpin, and G. D. Scholes, J. R. Soc. Interface **11**, 20130901 (2014).

[41] J. Schulze and O. Kühn, J. Phys. Chem. B **119**, 6211 (2015).

[42] R. Baer and R. Kosloff, J. Chem. Phys. **106**, 8862 (1997).

[43] C. P. Koch, T. Klüner, and R. Kosloff, J. Chem. Phys. **116**, 7983 (2002).

[44] D. Gelman and R. Kosloff, Chem. Phys. Lett. **381**, 129 (2003).

[45] D. Gelman, C. P. Koch, and R. Kosloff, J. Chem. Phys. **121**, 661 (2004).

[46] M. H. Lee and A. Troisi, J. Phys. Chem. **144**, 214106 (2016).

[47] V. May and O. Kühn, *Charge and Energy Transfer Dynamics in Molecular Systems* (Willey-VCH, Berlin, 2011), 3rd ed.

[48] C. P. Koch, T. Klüner, H.-J. Freund, and R. Kosloff, J. Chem. Phys. **119**, 1750 (2003).

[49] G. Herzberg and E. Teller, Z. Phys. Chem. B **21**, 410 (1933).

[50] H. J. Kupka, *Transitions in Molecular Systems* (Wiley-VCH, Weinheim, 2010).

[51] R. P. Fornari, J. Aragó, and A. Troisi, J. Chem. Phys. **142**, 184105 (2015).

[52] A. Troisi, A. Nitzan, and M. A. Ratner, J. Chem. Phys. **119**, 5782 (2003).

[53] S. Mukamel, *Principles of Nonlinear Optical Spectroscopy* (Oxford, New York, 1995).

[54] A. Kell, X. Feng, M. Reppert, and R. Jankowiak, J. Phys. Chem. B **117**, 7317 (2013).

[55] M. K. Lee and D. F. Coker, J. Phys. Chem. Lett. **7**, 3171 (2016).

[56] C. Kreisbeck, T. Kramer, M. Rodríguez, and B. Hein, J. Chem. Theory Comput. **7**, 2166 (2011).

[57] H. Tal-Ezer and R. Kosloff, J. Chem. Phys. **81**, 3967 (1984).

[58] R. Kosloff, Annu. Rev. Phys. Chem. **45**, 145 (1994).

[59] C. Leforestier, R. H. Bisseling, C. Cerjan, M. D. Feit, R. Friesner, A. Guldberg, A. Hammerich, G. Jolicard, W. Karrlein, H.-D. Meyer, et al., J. Comput. Phys. **94**, 59 (1991).

[60] J. M. Womick, S. A. Miller, and A. M. Moran, J. Chem. Phys. **133**, 024507 (2010).

[61] J. M. Womick, B. A. West, N. F. Scherer, and A. M. Moran, J. Phys. B: At. Mol. Opt. Phys. **45**, 154016 (2012).

[62] J. M. Womick and A. M. Moran, J. Phys. Chem. B **113**, 15747 (2009).

[63] J. M. Womick and A. M. Moran, J. Phys. Chem. B **113**, 15771 (2009).

[64] J. Aragó and A. Troisi, Adv. Funct. Mater. **26**, 2316 (2016).

[65] N. Renaud, M. A. Ratner, and V. Mujica, J. Chem. Phys. **135**, 075102 (2011).

[66] P. Rebentrost, R. Chakraborty, and A. Aspuru-Guzik, J. Chem. Phys. **131**, 184102 (2009).

[67] Y. Jing, R. Zheng, H.-X. Li, and Q. Shi, J. Phys. Chem. B **116**, 1164 (2012).

[68] M. K. Lee, P. Huo, and D. F. Coker, Annu. Rev. Phys. Chem. **67**, 639 (2016).

[69] M. Rätsep and A. Freiberg, J. Lumin. **127**, 251 (2007).

[70] The reorganization energy was obtained by integrating spectral density provided in ref.[55]